Science of the Total Environment 847 (2022) 157544

Contents lists available at ScienceDirect

Science of the Total Environment

journal homepage: www.elsevier.com/locate/scitotenv

Mining minerals and critical raw materials from bittern: Understanding metal ions fate in saltwork ponds

F. Vicari [a], S. Randazzo [b,*], J. López [c,d], M. Fernández de Labastida [c,d], V. Vallès [c,d], G. Micale [b], A. Tamburini [a,b], G. D'Alì Staiti [f], J.L. Cortina [c,d,e,*], A. Cipollina [b]

[a] ResourSEAs srl, Palermo, Italy
[b] Dipartimento di Ingegneria, Università di Palermo (UNIPA), Palermo, Italy
[c] Chemical Engineering Department, UPC-BarcelonaTECH, Barcelona, Spain
[d] Barcelona Research Center for Multiscale Science and Engineering, Barcelona, Spain
[e] Water Technology Center (CETaqua), Cornellà de Llobregat, Spain
[f] Sosalt SpA, Trapani, Italy

HIGHLIGHTS

- Original experimental information was collected in real saltworks (Sicily, Italy).
- A complete characterization of brines and solids from the ponds was carried out.
- For the first time, PHREEQC Pitzer code database was extended to the trace elements.
- The fate of major & minor elements along the ponds was effectively predicted.
- Saltworks bittern potential for critical raw materials recovery was evaluated.

GRAPHICAL ABSTRACT

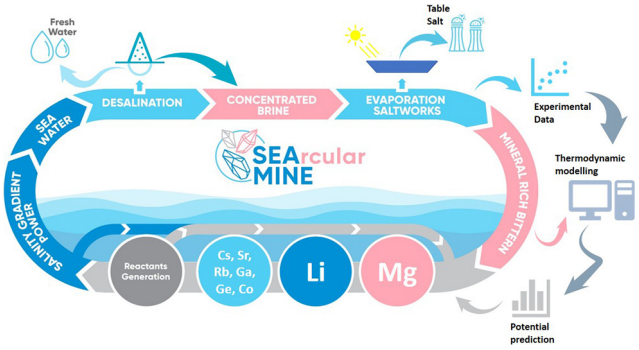

ARTICLE INFO

Editor: Jurgen Mahlknecht

Keywords:
Critical raw materials
Brine
Saltworks
Trace elements
PHREEQC
Pitzer

ABSTRACT

Seawater represents a potential resource for raw materials extraction. Although NaCl is the most representative mineral extracted other valuable compounds such as Mg, Li, Sr, Rb and B and elements at trace level (Cs, Co, In, Sc, Ga and Ge) are also contained in this "liquid mine". Most of them are considered as Critical Raw Materials by the European Union. Solar saltworks, providing concentration factors of up-to 20 to 40, offer a perfect platform for the development of minerals and metal recovery schemes taking benefit of the concentration and purification achieved along the evaporation saltwork ponds.

However, the geochemistry of these elements in this environment has not been yet thoroughly evaluated. Their knowledge could enable the deployment of technologies capable to achieve the recovery of valuable minerals. The high ionic strengths expected (0.5–7 mol/kg) and the chemical complexity of the solutions imply that only numerical geochemical codes, as PHREEQC, and the use of Pitzer model to estimate the activity coefficients of the different species in solution can be adopted to provide valuable description of the systems.

In the present work, for the first time, PHREEQC Pitzer code database was extended to include the target minor and trace elements using Trapani saltworks (Sicily, Italy) as a case study system. The model was able to predict: i) the purity in halite and the major impurities contained, mainly Ca, Mg and sulphate species; ii) the fate of minor components as B, Sr, Cs, Co, Ge and Ga along the evaporation ponds. The results obtained pose a fundamental step in critical raw materials mining from seawater brine, for process intensification and combination with desalination.

* Corresponding authors.
E-mail address: jose.luis.cortina@upc.edu (J.L. Cortina).

http://dx.doi.org/10.1016/j.scitotenv.2022.157544
Received 29 March 2022; Received in revised form 5 July 2022; Accepted 17 July 2022
Available online 22 July 2022

1. Introduction

Seawater contains large quantities of valuable minerals (3.3 % *w*/w), most of which are largely used in our society. The vast majority of the known elements can be found in seawater although many are at very low concentrations (Loganathan et al., 2017). The main elements which make up 99.9 % of the salts content in decreasing order are: $Na^+ > Mg^{2+} > Ca^{2+}$, $K^+ > Sr^{2+}$ (for cations) and $Cl^- > SO_4^{2-} > HCO_3^- > Br^- > BO_2^- > F^-$ (for anions) (Millero et al., 2008). Only a few minerals, the ones in high concentrations, are currently mined from the sea: NaCl as halite, extracted since ancient times for human consumption (Bardi, 2010), magnesium sulphate and bromide salts (Macedonio and Drioli, 2017). Land-based mining industries need to face the depletion of high-grade ores, while low-grade ores exploitation may lead to high water and energy demand associated with environmental concerns and increased complexity (Spooren et al., 2020). For this reason, seawater is regarded as a possible alternative for the production (European Commission, 2020).

Seawater and seawater brines exploitation have drawn much attention for the potential extraction of raw materials and energy (Cipollina et al., 2015). Indeed, seawater is rich in some compounds which are very scarce and expensive in their land-based form, such as alkaline/alkaline-earth metals (e.g. Li, Rb, Cs, Sr) and transition/post-transition metals (e.g. U, In, Sc, V, Co, Ga, Ge). Many of these elements are included in the EU Critical Raw Materials (CRM) list, grouping natural assets classified as fundamental for the wealth of the socio-economic structure of Europe (European Commission, 2020). A notable example of the interest in strategic minerals extraction from seawater is represented by uranium whose extraction is actively studied from the 80s in Japan (Hirotsu et al., 1986) and still feed the interest in USA from the last decade (Anirudhan et al., 2019; Hirotsu et al., 1986). Although new advances in concentration and separation technologies were accomplished, energy requirement for their extraction is often reported to be very high (Pramanik et al., 2020), especially for those in the lower part of the range (e.g. μg/L) (Bardi, 2010).

Elements as lithium, boron, strontium, vanadium, scandium, indium, germanium, and gallium represent important needs for the European Economy. Significant is the case of Rb, considered to be relevant to the development of quantum computing technology (Wang et al., 2021).

In this scenario, a costs-effective solution might be to exploit the concentration process already occurring in saltworks, leading to high concentrated brine called “bittern”. Table salt production in saltworks is an ancient industrial practice representing an effective example of integration of human activities and wildlife protection often resulting in protected areas in the framework of environmental protection initiatives such as Natura 2000 (e.g. in (Cipollina and Micale, 2016; Coelho et al., 2014; Glavaš et al., 2018; Sainz-López et al., 2019)). About one-third of the global table-salt production is manufactured in solar saltworks (Davis, 2013), where natural evaporation of seawater using the renewable energy (e.g. solar energy) leads to recover table-salt by fractional precipitation in several ponds. It is a simple and effective method with the drawback of being land-intensive, as the evaporation ponds need to be shallow. This method has been employed for thousands years to produce common table-salt from seawater worldwide (Loganathan et al., 2017).

With the aim of recovering very high purity sodium chloride (NaCl), the key to success of saltworks is to carefully control minerals precipitation collecting them in different ponds. Along the sequence of evaporation and concentration stage, calcium and sodium salts precipitate leaving bitterns in which trace elements concentration increases up to 20–40 folds than in seawater. Reusing these streams by dilution in the brines in the early stages of the process cannot be repeated indefinitely and carrying them back into a natural receiving water body in large quantity, nowadays, could represent a problem in terms of environmental impact (Cipollina et al., 2015). On the other hand, their treatment as a waste stream could dramatically affect sea-salt production economic sustainability.

Conversely, recovery of valuable minerals from bitterns could provide a double benefit, reducing environmental concerns and, at the same time, generating an additional profit for saltworks owners. The EU funded project “Circular Processing of Seawater Brines from Saltworks for Recovery of Valuable Raw Materials” (SEARcularMINE) proposes to treat bitterns to recover several valuable minerals - Mg, Li, Rb, Cs, Sr, Co, Ga, Ge- with a circular approach perspective (SEArcularMINE, 2021). The project aims at bringing this tradition to the 21st century by equipping salterns with modern tools that can give to mankind raw materials which are as valuable as table salt has been for centuries while maintaining the same kind of integration with the environment. Indeed, the upstream integration of desalination to the traditional saltworks is proposed within the project, aiming at providing freshwater to the local communities and additional saturated brine to the saltworks, increasing their productivity. Moreover, this circular approach has the potential to maximize resources recovery efficiency and economic viability, including on-site generation of reactants and electricity from salinity gradients.

Unveiling the laws governing fractionated separation of the impurities in the different ponds could allow for the definition of a design approach that can be adapted to other industrial processes for brine management and treatment.

When the natural degradation of organic matter occurring in natural environments was recognized, biological treatment of wastewater was postulated, which in time was intensified and industrialized. Similarly, a proper description of saltworks operation through governing equations could be of inspiration for designing new circular brine management strategies resulting in waste and energy consumption minimization and value production.

Other authors have already characterized saltworks evaporitic environment, mainly with the scope of predicting table salt production also in combination with desalination (Cipollina et al., 2012; Sainz-López et al., 2019). However, a complete description of mineral phases extraction was beyond the scope of these studies.

Conversely, such a detailed description was adopted by Hajbi et al. studying the crystallization sequence of reverse osmosis (RO) brine during isothermal and isobaric evaporation (Hajbi et al., 2010). Berton rules and multiple phase-diagrams can be used to describe the crystallization path of calcium, sodium and magnesium salts (chloride and sulphates) (Hajbi et al., 2010). However, the complexity of this method can become overwhelming if the number of elements analyzed is extended to include the full list of trace elements of potential interest in the brine. To address the complexity of large multicomponent mixtures at high ionic-strength, semi empirical thermodynamic models were developed for the computation of the activity coefficients and the mineral saturation indexes (SI). Among them the models developed by Pitzer and Simonson have been widely tested and recognized as a reliable tool (Hajbi et al., 2016; Parkhurst and Appelo, 2013; Pitzer, 1981; Simonson and Pitzer, 1986).

While much work has been done in the characterization of other evaporitic environments (Gao et al., 2020; Li et al., 2019, Li et al., 2016), few studies can be found focused on real saltworks, with full scale applications for the prediction of the major minerals crystallization components in saltworks (Kasedde et al., 2014; Vančina et al., 1997). In this context, PHREEQC, embedding Pitzer model, which has been proven to be an effective for other evaporitic environment modelling (Golan et al., 2016), might represent an advantage for saltworks modelling.

In the present work, PHREEQC code using Pitzer approach was used to describe the fate of both major and minor elements along the twelve ponds of the complex model system of the Trapani saltworks (Sosalt spa, Italy).

In a large-scale sampling campaign, the saltworks was characterized in terms of structure, operation, composition of the brines along the twelve ponds as well as the composition of sludge and salts accumulated on basins bead using chemical, mineralogical and morphological analytical techniques.

Information generated from the analytical and operation data were used to build a predictive tool based on PHREEQC to describe i) the variation of the concentration of major and minor species in the brines; ii) the composition of the mineral phases expected due to the combination of the evaporation, precipitation and crystallization processes. Model prediction was compared with analytical evidence from both liquid and solid samples obtained. The results obtained pose a fundamental step in critical raw

materials mining from seawater brine, for process intensification and combination with desalination.

1.1. Model site description: Trapani saltworks

Trapani saltworks, located on the west coast of Sicily, in the heart of Mediterranean Sea, was selected as model site for evaluation of the platform for the development of metal and minerals recovery schemes. This area has been an important center for the production of salt from seawater since Phoenician occupation (750 BCE), due to the ideal weather-climatic and geomorphological conditions of the coastal area for saltworks setting-up (Cipollina et al., 2012).

The "Sea Salt of Trapani" is produced by using the typical method of fractional precipitation of the impurities and undesired minerals contained in seawater, cured by experienced saltworkers. The water flows through several order of ponds of increasing in density and ions concentration. In particular, adopting the technical Baumè density scale (Bè) familiar to saltworkers, the salt density grows from the initial value of 3.5°Bè (seawater) up to the saturation point of sodium chloride (25.7°Bè).

A scheme of the salt production process is represented in Fig. 1, while in Fig. 2 is reported the layout of the main Sosalt saltworks, where also sampling points are indicated.

In the typical design (Fig. 1), the ponds can be grouped in four orders according to the different evaporation stages of the production process, each order being characterized by a well-defined density range:

- Evaporation zone I, "cold ponds" or "first-entry ponds"(P1-P3 in Fig. 2), where seawater is received during tidal influxes or forcibly through dewatering pumps or windmills when natural power supply is not practicable. The density raises up from 3.5°Bè to 5–6°Bè. It covers 20–25 % of the total saltwork surface, with a depth up to 100 cm;
- Evaporation zone II, "driving ponds" (P4-P6 in Fig. 2), which are fed by the cold ones. The density grows from 5 to 6°Bè to 9–11°Bè. Their total surface covers about 30 % of the total saltwork surface. The pond depth is here reduced to <50 cm. In addition to the transition metals (usually present as trace elements), carbonates can precipitate;
- Evaporation zones III and IV, "hot ponds" or "evaporative ponds" (P7-P10 in Fig. 2), made by several small and shallow (<40 cm) ponds, covering at least 35 % of the total saltwork surface. Here, the area is segmented into groups of three or four different ponds fed in series with the water coming from the driving ponds. Carbonates and sulphates precipitate are expected to reach the saturation point and then they precipitate before leaving the last ponds. This is very important to carefully control this process as it can allow to obtain a sea-salt product purity of >98 % without any further purification process. In the last pond, called "*sentina*", the water reaches the saturation of halite (25.7°Bè). Each *sentina* serves a small group of crystallizing ponds;
- Crystallizers, "crystallizing ponds" (P11-P12 in Fig. 2), where table-salt crystallizes. They are very shallow (10–25 cm) with very flat floor. They account for maximum of 15 % of total saltwork surface. During the hot season, they are fed more twice or three times per week in order to compensate for volume loss due to the evaporation and keep brine density below 30°Bè. In this way, Mg salts precipitation is controlled, thus enhancing the quality of the produced salt. An estimated evaporation rate of almost 1 cm/day in the summer season implies that a crust of about 10 cm is grown in 45 days.

The production cycle is repeated with yearly frequency. Saltwork feeding starts at the end of April, when the evaporation rate is sustained enough to counterbalance eventual rainfall (<100 mm total rainfall from May to September).

2. Material and methods

2.1. Sampling campaign

Liquid and solids samples from ponds 1 to 12 (Fig. 2) were collected in July 2020. For the liquid samples a 200 mL volume was withdrawn from the ponds surface and from the pond borders using sterile sample holders. Solid samples were taken from the bottom of the ponds, using a plastic spatula and stored in a 100 mL sample holder, from the same point were the liquid samples were taken. Samples were immediately sealed and sent to the laboratories (BarcelonaTECH, Barcelona, Spain) for chemical analysis and characterization. Samples were stored at 4 °C.

2.2. Analytical techniques

2.2.1. Liquid sample analysis

Liquid samples have been characterized by using different analytical techniques according to the estimated elements concentration. Ion chromatography (Dionex ICS-1000 and ICS-1100) with the cation-exchange IONPAC® CS16 anion-exchange IONPAC® AS23 columns was used to determine the concentration of major cations and anions in solution. The mobile phases were a 0.03 mol/L CH_3SO_3H solution for the cation-exchange column and a mixture of 45 mmol/L Na_2CO_3 and 0.8 mmol/L $NaHCO_3$ solution for the anion-exchange column. Inductively Coupled Plasma Mass Spectrometer (7800 ICP-MS from Agilent Technologies) and Optical Emission Spectrometer (5100 ICP-OES from Agilent Technologies) were used to determine the concentration of the minor elements in solution. Samples were previously diluted, acidified with 2 % HNO_3 and filtered with 0.22 μm syringe filters.

The Total Inorganic Carbon content (TIC) was determined using a TOC-V CPH (Shimadzu). Samples were previously diluted and filtered with 0.22 μm syringe filters. From the TIC measurements, the alkalinity content was estimated.

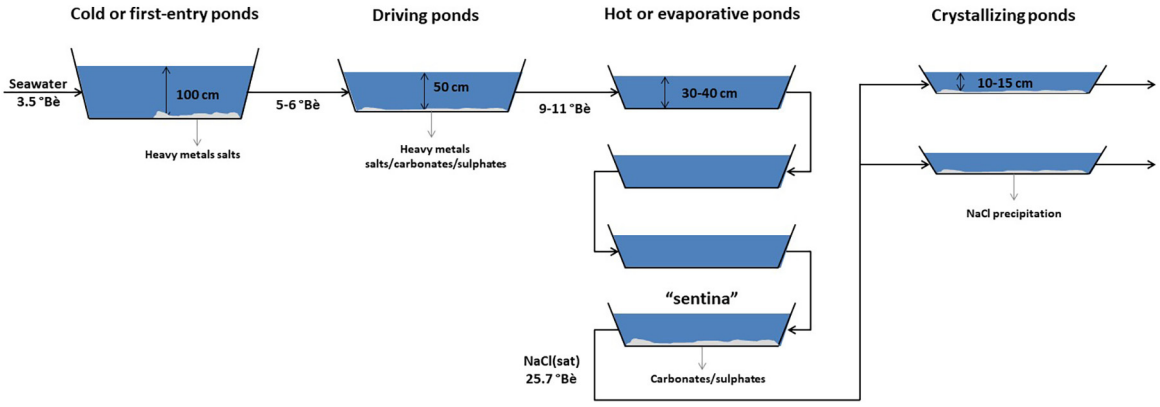

Fig. 1. Description of the salt production process in Trapani saltworks (Italy) where the "Sea Salt of Trapani" is produced.

Fig. 2. Overview of the Trapani saltworks ponds considered as the model platform used for the development of metal and minerals recovery schemes in this work.

The pH of the samples was measured by using a pH-glass electrode (GLP 22, Crison) calibrated with standard reference solutions of pH 4.02 and 7.00 as a first approximation. Conductivity measurements were performed with a Crison GLP 31 EC. The density was measured using hydrometers of different operating range, from 0.9 to 1.3 g/cm^3, with a resolution of 0.001 g/cm^3.

2.2.2. Solid samples analysis and characterization

Solids samples from the ponds were pre-treated before the analysis following different protocols as a function of the water solubility of the main minerals possibly present. Expected mineral phases were deduced from the knowledge provided by the Trapani saltworkers and from the reviewed literature (e.g. (Vančina et al., 1997)). Samples from ponds 1 to 8 were washed several times with water until no chloride was detected in the washing water by using a $AgNO_3$ solution as visual indicator (i.e. no precipitation of AgCl(s) was detected). In this group of ponds expected minerals are calcium and magnesium sulphates or carbonates and silicates as some presence of organic matter containing solids, all of them with low solubility in water (e.g. <1 mg/L). Solid samples from ponds 9 to 12 were washed with acetone as the main expected components are soluble mineral phases of chlorides and sulphates of sodium, potassium or magnesium. After washing, in both cases samples were dried at 40 °C for 48 h prior to their analysis to remove humidity (> 99 %). Then, samples were digested by dissolving 0.1 g of dried solid in 10 mL of HNO_3 (65 %) and diluted to analyze their chemical composition by ICP-MS and ICP-OES. Additionally, the morphology of the samples was obtained by using Scanning Electron Microscopy (JEOL JSM- 7001F) at an acceleration voltage of 20.0 kV for secondary-electron imaging (SEI) and backscattered imaging for composition (COMPO) after being coated with an alloy of Pt/Pd.

Besides, in order to identify the crystalline phases, x-ray diffraction (XRD) analysis were carried out after grinding the sample. A Bruker D8 Advance A25 x-ray diffractometer was used with a Bragg-Brentano configuration θ-θ. The equipment has a Cu x-ray tube, which allows to work up to 40 kV and 40 mA. The spectrum was recorded from 15° to 60° with steps of 0.020°. The identification of mineral phases was performed with EVA software (Bruker).

2.3. Geochemical modelling of the saltwork-pond operation by using PHREEQC and the Pitzer database

For the first time PITZER database was extended to elements conventionally neglected for their low contents (mg/kg to μg/kg) as Sr, Cs, Rb, Co, Ga and Ge and considered in the new world scenario of identification of alternative mineral resources. Concerning B and Li, some new constants were added to the existing ones (see Tables S1 in the supplementary information file). From the initial composition of the seawater fed into the saltworks and taking into account the information of the evaporation ratios achieved along the different ponds, the variation of major and minor solutes concentrations in both brine and sludge accumulated on the saltwork bed was simulated with the PHREEQC (version 3.6.2) numerical code (Parkhurst and Appelo, 2013). A temperature of 27 °C was assumed for running the simulations. In particular, this value was taken from ISPRA (Istituto Superiore per la Protezione e la Ricerca Ambientale) website referring to the weather conditions in Italy in 2019. Due to the high-salinity of the solutions, the Pitzer database was used. This database only includes correlation coefficients for most commonly studied elements (e.g. alkalinity, Na, K, Ca, Mg, SO_4 and Cl), whereas trace elements are traditionally excluded from simulations. Therefore, the Pitzer database was extended with values extracted from the literature in order to include them (Kolpakova and Gaskova, 2018). Equilibrium with atmospheric CO_2 was also imposed (log $pCO_{2(g)} = -3.5$). Additionally, mineral phases precipitated along the evaporation process were considered to be non-dissoluble (as they were harvested). Predicted concentrations of the ionic species in the brines of the different ponds were plotted as a function of water evaporated. The evaporation ratio was estimated on the base of the measured brines density values. It should be mentioned that in the last ponds of the saltwork, blending options of bitterns is performed to achieve the required control on the $NaCl_{(s)}$ crystallization (i.e. ponds 11 and 12). Pitzer

coefficients and equilibrium data are shown in S1 paragraph in the supplementary information file.

3. Results and discussion

3.1. Characterization of Trapani saltwork ponds brines

The main physicochemical properties of the brines of the twelve ponds of the Trapani saltworks, i. e. density, pH and concentration of cations and anions of interest, were measured. Results are reported in Table 1 organized according to the different evaporative stages (see Section 2).

Results show different kinds of behavior for the analyzed parameters and ions: i) those considered conservatives, whose concentration increases with the increase of the evaporation degree under a linear dependence, and ii) those not having a conservative behavior along the saltwork due to the precipitation of mineral phases when the saturation is reached. For example, of relevant importance is the variation of Ca(II) concentrations, increasing from 0.4 g/kg up to 1.2 g/kg in pond P6, and later being reduced to values below 0.17 g/kg in pond 12. This reduction of Ca(II) by the natural operation of the pond is of crucial relevance for the potential valorization of other cations as Mg, Sr or trace elements as Li, B, Cs, Ga, Rb or Ge. Focusing on trace elements, the group of Li, Sr, Rb and B, showing conservative behavior, can be identified as potentially attractive to develop recovery processes from the brines generated after crystallization of NaCl and after the recovery of Mg(II) in the form of $Mg(OH)_{2(s)}$ as it has been postulated elsewhere (Cipollina et al., 2015).

Finally, Cs, Co, Ge and Ga constitute the group with a concentration very close to the limit of detection, as for Cs (0.001–0.002 mg/kg) or even below their detectability as for Co and Ge (< 0.002 mg/kg in both cases). In particular, Cs concentration shows a flat trend not following the expected concentration dependence due to evaporation, whereas Ga was found to have a conservative behavior in the first eight ponds and then slowly decreasing to approach the limits of detection in the last evaporation ponds.

It should be noted how, independently from their belonging group, many elements seem to have a local minimum in pond 11, where the concentration is lower than what can be seen for both pond 10 and 12. This is true for major ions such as Mg, K and SO_4^{2-}, but also for minor elements such as B and trace elements such as Li. This behavior can be explained by the flow-blending practiced in Trapani saltworks that will be better discussed below.

Fig. 3 shows the morphology of the samples collected along the saltwork ponds by providing SEM images for ponds 1,5,7,9,10 and 12, while EDS spectra can be find in S2 in the supplementary information file. Samples from ponds 1 to 5 showed a high presence of silicates (large smooth surface in P1) with a small presence of organic containing solids with an amorphous morphology as it could be seen in in samples of P5. Noteworthy, sample from pond 5 showed the presence of microorganisms (rod-shaped, striped in the center of P5). The biological activities in solar saltworks has mainly been studied in relation to its importance for table-salt production (Davis, 2013), but it is known to be relevant also for the polishing stages of cations as Ca(II) removed from the brine by precipitation of calcium carbonates and or calcium sulphates (Zhu and Dittrich, 2016).

By EDS analysis, it was observed for samples of P7, the presence of long narrow crystal solids characterized by the presence of Ca, S and O, suggesting the presence of calcium sulfate (i.e. gypsum as confirmed latter by XRD). Additionally, the presence of crystals containing Sr in P9 and P10 was also highlighted in the form of small needles and large flowers type of precipitated crystals, typical morphologies of strontium sulphate (e.g, celestite). Finally, samples from the last pond were characterized by the presence of cubic crystals, typical of $NaCl_{(s)}$ but on the surface of these very large crystals gypsum and magnesium sulphate impurities can be recognized (large stick and small conglomerate in the red circle of P12).

Solid samples have also been analyzed by XRD and the main mineral phases identified are shown in Table 2.

It was observed the presence of silicates (e.g. quartz, illite and kaolinite) which are the main solar-pond soil or basement components of the different ponds. Moreover, XRD allowed to identify the mineral phases that precipitate during the crystallization process, such as calcite and aragonite (from seawater intake 0 to pond 9), gypsum (from ponds 6 to 11) and halite (from ponds 1 to 12).

Neither chemical analysis by FESEM-EDAX nor XRD were providing relevant information of the presence of trace elements on the sludge samples collected along the ponds, apart those from P2 and P3 samples where some particles containing Cs or Sr were identified. For this reason, acid digestion of the solids was performed to determine if trace elements precipitated, co-precipitated or were removed by sorption processes along the evaporation ponds. Results on the trace element content ($\mu g/g_s$) on the sludge samples of P1-P12 are summarized in Table 3.

It can be observed that the main element that precipitated was the Sr, especially in the ponds prior to NaCl crystallization (ponds 9–11) with a content of 2.7–3.1 mg/g. The other elements remained below 10 μg/g, except B, which moved between 10 and 50 μg/g. When focusing on the elements at trace levels (i.e. Li, Co, Ga, Ge, Rb and Cs), the higher values were found on the sludge collected in the cold and evaporation ponds (i.e. 1–6). As discussed previously, the main mineral phases identified by

Table 1
Elemental composition, density, total inorganic carbon content (TIC) and pH in Trapani (IT) saltworks ponds (ponds numbering, P1-P12, refers to the scheme reported in Fig. 2).

Element		Cold ponds			Driving ponds			Hot ponds				Cryst. ponds	
		P1	P2	P3	P4	P5	P6	P7	P8	P9	P10	P11	P12
Density (kg/L)		1.016	1.025	1.027	1.039	1.049	1.073	1.118	1.142	1.210	1.216	1.212	1.220
pH		7.89	8.25	7.67	8.02	7.73	8.01	7.94	7.85	7.43	7.44	7.47	7.32
g/kg	Na	10.37	14.09	15.96	21.61	23.04	32.21	51.89	58.66	80.72	78.58	78.41	68.42
	K	0.42	0.48	0.54	0.75	0.82	1.21	2.16	2.52	3.74	4.14	4.03	5.90
	Mg	1.48	1.64	1.84	2.53	2.76	3.89	6.95	8.01	11.87	13.26	12.73	18.09
	Cl	20.20	24.18	27.48	38.77	41.55	59.76	101.45	116.35	165.66	164.74	163.27	161.65
	SO_4^{2-}	2.95	2.90	3.21	4.42	4.81	7.35	10.89	11.79	17.15	19.29	18.39	28.09
	Br	0.07	0.08	0.09	0.12	0.13	0.19	0.35	0.40	0.61	0.67	0.65	0.94
mg/kg	Li	0.21	0.27	0.33	0.37	0.37	0.59	0.90	1.01	1.50	1.61	1.46	2.22
	B	4.37	5.16	5.80	8.48	9.14	14.03	24.90	28.44	41.34	45.11	44.95	64.69
	Sr	8.09	9.40	10.61	13.92	14.96	21.82	28.30	29.36	26.58	26.16	28.73	23.38
	Ca	437.48	501.74	552.11	722.85	789.45	1147.19	850.56	653.25	242.95	217.49	230.53	164.85
	Co	<DL[a]	<DL	<DL	<DL	<DL	<DL	<DL	<DL	<DL	<DL	<DL	<DL
	Cs	0.002	0.003	0.002	0.002	0.002	0.001	0.001	0.001	0.001	0.001	0.001	0.001
	Ga	0.003	0.004	0.006	0.009	0.010	0.011	0.012	0.013	0.005	0.004	0.005	0.000
	Rb	0.12	0.15	0.17	0.23	0.25	0.36	0.59	0.66	0.93	0.98	0.99	1.38
	Ge	<DL[2]	<DL	<DL	<DL	<DL	<DL	<DL	<DL	<DL	<DL	<DL	<DL
	TIC	36.85	31.79	39.45	31.25	31.04	27.60	32.16	33.47	40.50	41.93	43.50	54.33

[a] DL(Co) = 0.002 mg/kg, [2]DL(Ge) = 0.002 mg/kg.

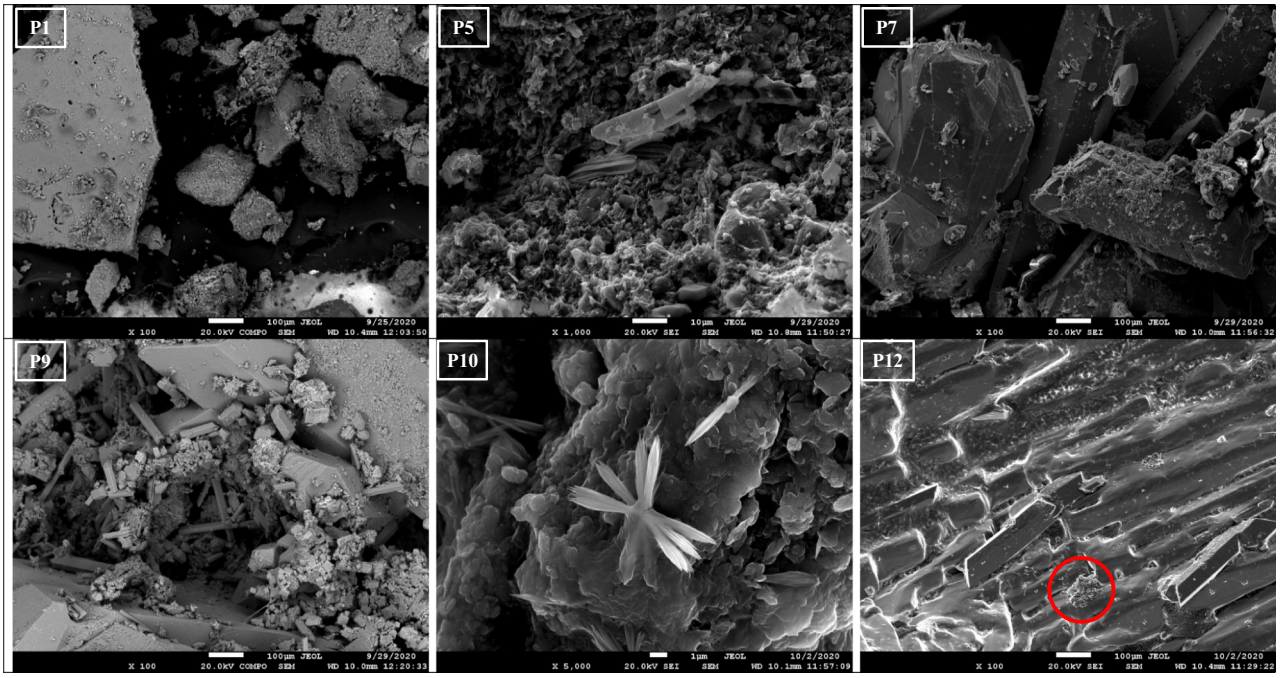

Fig. 3. SEM images of the solids collected at the bottom of selected ponds in Trapani (IT) saltworks ponds using 20 keV secondary-electron imaging. The red circle in P12 shows an agglomerate containing high concentration of magnesium, sulphates and potassium.

XRD, although the presence of other amorphous or at low fraction phases, it could not be discarded that two main families of minerals could be identified: i) carbonates as calcite, aragonite, dolomite and ankerite, and ii) silica based minerals as quartz and aluminosilicates as illite, kaolinite, microcline and montmorillonite.

Carbonate based minerals have been described as the sink of many divalent transition (e.g. Cd, Ni, Co, Pb) ions present at trace levels in seawater and incorporated onto the structure of carbonates minerals (Lorens, 1981) or adsorbed on their surfaces through complexation reactions (Reeder, 1996). The presence of Co could be associated to these two mechanism although it could not be discarded the presence as $Co(OH)_2(s)$. In the case of Li(I), Rb(I) and Cs(I), their incorporation on any aluminosilicate mineral is the most plausible hypothesis as the family of minerals are the most common sources used for their exploitation. For example, for the case of Li, the main mined minerals are spodumene ($LiAl(SiO_3)_2$), lepidolite, $K(Li,Al)_3(Al,Si,Rb)_4O_{10}(F,OH)_2$ and petalite ($LiAlSi_4O_{10}$) (Bae and Kim, 2021). For the case of Rb(I), it occurs naturally in the minerals leucite ($KAlSi_2O_6$), pollucite ($(Cs,Na)_2Al_2Si_4O_{12}{\cdot}2H_2O$), carnallite ($KMgCl_3{\cdot}6(H_2O)$), lepidolite and zinnwaldite ($KLiFeAl(AlSi_3)O_{10}(OH,F)_2$), and for the case of Cs(I), it is also found as trace in some of the minerals described for Li(I) and Rb(I) (Butterman and Reese, 2003). It should be mentioned

Table 3
Composition of trace elements (μg/g$_s$) in the solids collected in the different ponds in Trapani (IT) saltworks (DL(detection limits)).

Pond	Elemental concentration in solid samples (μg/g$_s$)							
	Li	B	Co	Ga	Ge	Rb	Sr	Cs
0	3.09	51.31	3.22	2.39	0.58	5.09	1106.1	0.28
1	1.50	14.35	1.86	1.24	0.48	1.50	526.66	0.08
2	4.07	27.00	5.59	4.40	0.77	5.02	669.34	0.20
3	2.46	38.77	2.21	2.72	0.53	2.65	1002.4	0.11
4	4.94	22.18	5.24	7.46	0.83	7.01	787.34	0.21
5	6.20	51.37	4.19	8.03	0.52	5.54	1777.2	0.15
6	3.58	33.20	2.86	7.60	0.37	3.53	1442.3	0.10
7	0.79	14.04	0.32	0.80	0.03	0.41	1001.2	<DL
8	1.20	21.05	0.37	2.53	0.08	0.83	1497.1	0.02
9	1.82	33.54	0.37	4.84	0.08	1.14	2790.1	0.02
10	1.20	21.32	0.13	2.81	<DL	0.70	2861.5	<DL
11	1.42	23.79	0.15	3.24	0.06	0.62	3088.8	<DL
12	0.69	7.78	<DL	0.04	<DL	0.10	18.29	<DL
Avg.	2.54	27.67	2.21	3.70	0.39	2.63	1428.33	0.13

Table 2
Mineral phases identified by XRD in the solids of the different ponds in Trapani (IT) salworks.

Solid sample – ponds_	0	1	2	3	4	5	6	7	8	9	10	11	12
Calcite, syn – $CaCO_3$	✓	✓	✓	✓	✓	✓	✓		✓	✓			
Aragonite – $CaCO_3$	✓	✓	✓	✓	✓	✓	✓		✓				
Gypsum – $CaSO_4{:}2H_2O$							✓	✓	✓	✓	✓	✓	
Halite, syn – NaCl		✓	✓	✓	✓	✓		✓	✓	✓	✓	✓	✓
Quartz, syn – SiO_2	✓	✓	✓	✓	✓	✓	✓		✓	✓		✓	
Illite (K,H_3O) $Al_2Si_3AlO_{10}(OH)_2$	✓		✓			✓							
Kaolinite – $Al_2Si_2O_5(OH)_4$	✓	✓	✓	✓	✓	✓	✓						
Dolomite – $CaMg(CO_3)_2$	✓												
Microcline – $KAlSi_3O_8$		✓	✓										
Montmorillonite $Na_{0.3}(AlMg)_2Si_4O_{10}OH_2{:}6H_2O$					✓								
Ankerite – $Ca(Fe^{+2},Mg)(CO_3)_2$			✓			✓							
Calcite Mg-rich – $(CaMg)CO_3$							✓						

that it is also found in other minerals as pezzottaite ($CsLiBe_2Al_2Si_6O_{18}$) (Muuri et al., 2020). In most of the described cases, the contents of the three elements are below 1 % and their presence in the mineral is the substitution of other major components as Na and K. In any case, the heterogeneous distribution of trace elements within individual carbonate crystals (e.g. calcite) is a phenomenon commonly observed in natural and laboratory systems. Recently, Gabitov et al. (Gabitov et al., 2021) evaluated the elemental distribution by using partition coefficients of trace and minor elements (e.g. Li, B, Mg, and Sr) in calcite crystal faces along the mineral growth stages. Then, the presence of the mentioned trace elements in the carbonate mineral phases found could not be discarded.

Finally, for the case of Ga and Ge, as their solution chemistry is totally different in aqueous solutions, they tend to form hydroxy-acid species as $Ge(OH)_{4,aq}$ for Ge(IV) and $Ga(OH)_{3aq}$ and $Ga(OH)_4^-$ for Ga(III). In the case of Ge, its behavior in natural systems, although it behaves similarly to Si, Ge/Si ratios are fractionated by several processes in continental and marine environments (Barbier and Levy, 2010; Froelich et al., 1985). Then, it is expected to be associated to aluminosilicate phases, but there are different inorganic processes driven by enrichment of Ge in secondary clay minerals and/or iron oxy-hydroxides as well as other biogenic silica cycling (Pokrovsky et al., 2006). In the case of Ga, its sink in the natural systems is associated to sorption and complexation reactions with Al and Fe hydroxioxides as reported latter (see par. 3.3).

3.2. Simulation of pond performance and fate of trace elements by PHREEQC-Pitzer code

The PHREEQC simulation of the saltworks functioning was developed by using as input the composition of pond 1 (see Table 1), which can be assimilated to the seawater intake. Gradually a continuous subtraction or evaporation of water, as main process involved, leading to mineral saturation was adopted as calculation and simulation protocol of saltwork operation. A similar approach was proposed by Ayora et al. to describe the evaporation of Li reach inland saltworks in Chile (Gamazo et al., 2011; Marazuela et al., 2018). As it can be seen, a very good prediction of the concentration of major ions was obtained when compared with the measured values with a high correlation coefficient ($0.9 < R^2 < 0.99$) as reported in the Fig. S3 in the supplementary information file.

A singular characteristic of Trapani saltworks is the use of partial blending of the pond flows accessing the crystallization basins. Saltworkers routinely blend the water exiting from P10 with that coming from P7. The effect of this blending can be observed in Table 1 by analyzing the variation of in ions concentrations having conservative behavior. As already introduced, taking the example of lithium, the effect of mixing is apparent, noticing the constant increase of concentration from P1 to P10 up to 1.44 mg/kg and the drop recorded in P11 at 1.3 mg/kg (see Table 1). From the flow-rates mass balances a recirculation ratio (REC) can be defined by using (Eq. (1)):

$$REC = Q_{P7}/(Q_{P7} + Q_{P10}) \quad (1)$$

where Q_{P7} and Q_{P10}, are respectively the flow rates (kg/h) taken from pond 7 and pond 10 to form the inlet of pond 11.

On the base of the information acquired during the sampling campaign and the observed density variation, a REC value of 0.127 has been calculated. Accordingly, the simulation of the pond operation was carried using a REC value of 0.127.

3.2.1. Control parameters and brine composition variation along the water path

Density, probably the most important parameter monitored in saltworks, was investigated with the implemented model. In Fig. 4, the experimental values of density as a function of the amount of water evaporated are compared with those predicted by PHREEQC. A very good estimation of the measured density values has been obtained, providing also the description of the composition of the brine accessing the crystallization ponds (see in the Fig. S3 in the supplementary information file).

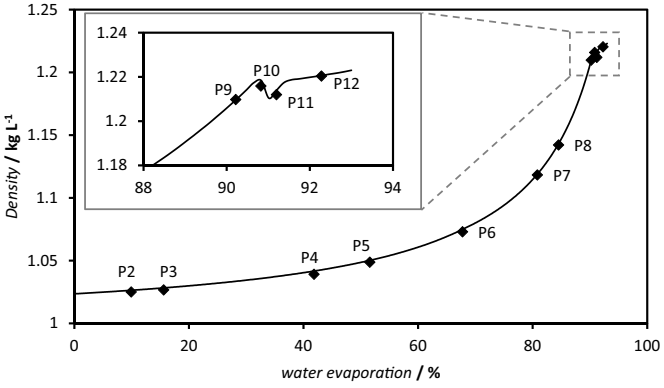

Fig. 4. Experimental (symbols) and modelling (lines) values for density as a function of the evaporation ratio in Trapani saltworks in the ponds.

In the inset of Fig. 4 (density variation as a function of the evaporation ratio), a focus on the last four ponds is given, showing a clear drop due to the abovementioned blending stages. The inset also highlights the change in density profile behavior after P11, a quantitative change in the slope of the function density versus evaporation extent, which can be attributed to sodium chloride crystallization in the form of halite.

As expected, the change in trend occurs at a density value of about 1.215 kg/L which corresponds to the abovementioned 25.7°Bè, obtained for a water evaporation ratio of about 91 %.

In addition to the density, also pH and alkalinity are commonly reported control parameters of the salt production process in saltworks as they are strictly related to carbonates equilibrium and crystallization, this last taking place especially in the so-called hot ponds and enduring up to the final crystallization ponds.

In Fig. 5, a comparison between experimental and modeled value of pH is presented.

During the experimental sampling campaign of summer 2020, pH was measured as described in the materials and methods section by using a pH-glass electrode calibrated with standard reference solutions. It is possible that this approach has led to the large deviations in pH measure observed in Fig. 5 in which this parameter seems to have important differences from a pond to another without a uniform trend, in opposition to what has been obtained with PHREEQC. Indeed, it was found that a more appropriated way of performing this kind of measure, minimizing liquid junction potential errors for high ionic strength solution is to add NaCl to standard NIST buffers solutions used for instrument calibration and assigning them corrected pH values using the Pitzer approach (Nir et al., 2014).

Fig. 5 also reports the alkalinity, in terms of $CaCO_3$ equivalents, as a function of the evaporation ratio, for both the simulation and the

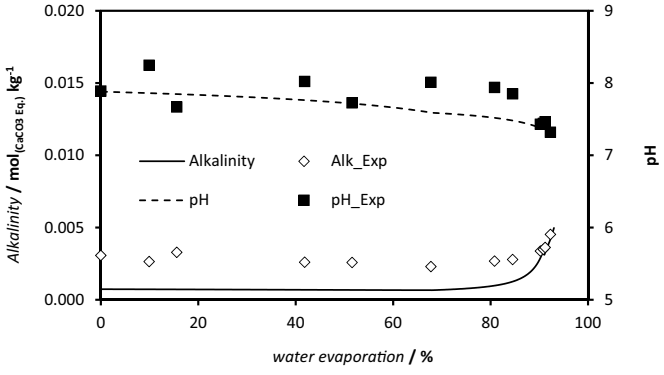

Fig. 5. Experimental (symbols) and modelling (lines) values for pH and alkalinity during evaporation in Trapani saltworks in the ponds.

experimental values measured along the campaign. In this case, a more reasonable behavior of the experimental values is here represented in agreement with the trend shown by the simulation. Noteworthy, for both alkalinity and pH the best agreement between the simulation and the experimental campaign is found in the last ponds, where their influence in the production process is maximum (see Fig. 5). As it has been described previously, micro-biological activity in saltworks pond could affect carbonate equilibria as they have been reported controlling the precipitation of calcium carbonates (Davis, 2013). These mechanisms affecting the global processes describing the variation of pH along the ponds could not be included in the PHREEQC modelling. In any case the good prediction provided indicates that these microbiological processes are having a more limited influence on last ponds bitterns pH values.

In Fig. 6A, major ions concentration values show an increasing trend for most of them with the increase of the evaporation ratio, thus replicating the concentration factor of water during evaporation. The exception is represented by sodium and chloride ions that stop their growth in correspondence to the same water evaporation percentage seen in Fig. 4 due to their precipitation as halite. Noteworthy, even if the beginning of halite precipitation was exactly predicted, the residual content in solution of sodium and chloride ions was slightly overestimated (~5 % lower). In Fig. 6B, minor ions concentrations are also reported. A good agreement was obtained for each minor ion, including calcium and strontium which precipitate in form of celestite before halite crystallization occurs as confirmed by the morphology of the crystals observed by EDS analysis reported above. Crystals were mainly composed by Sr, O and S that latter were not detected by XRD because their content on the solid analyses was below 0.5 % (*w*/w). Even though Macedonio and co-workers have already postulated a similar fate of strontium in reverse osmosis retentate using PHREEQC (Macedonio et al., 2013), this is the first time that such a comprehensive thermodynamic modelling unveils this mechanism in saltworks and using SEM images to confirm the prediction obtained (see Fig. 3, P10). However, the predicted residual concentrations in the bitterns were slightly lower than those measured experimentally, although the sulphate content profile was well predicted as it could be seen in Fig. 6A. Probably, an effort on the review of the equilibrium solubility data and Pitzer data for Sr is required.

3.2.2. Variation of minerals and table-salt composition along the crystallization path

In agreement with the state of the art knowledge on evaporitic environments (Bąbel and Schreiber, 2014), and with the XRD results shown in Table 2, calcium salts are first precipitated in the form of carbonates ($CaCO_{3(s)}$) as calcite and aragonite and then identified and as calcium sulphate in gypsum ($CaSO_4{:}2H_2O_{(s)}$) (see Fig. 7). Calcite and aragonite precipitation occurs already in the cold ponds but it acquires a significant magnitude only when the concentration factor (CF) reaches values of about 4 in the hot ponds (pond 7), which is also the onset for gypsum deposition. Formation of calcite in brines having large concentration of Mg(II) as Sr(II) has been described as a process kinetically controlled by the partial substitution of Ca(II) ions by Mg(II) and Sr(II). The substitution of Ca(II) by Mg(II) is more favored for the crystal structure of aragonite than for the crystal structure of calcite.

Noteworthy, when gypsum starts crystalizing, the XRD analysis highlights the absence of calcite in the solids (see Table 2, pond 7). This can be attributed to the local undersaturation of calcium carbonate caused by the sudden removal of large quantities of Ca(II) with gypsum deposition. As its rate of crystallization grows fast, calcite grows slow, and suddenly they drop together when halite starts precipitating (CF ≈ 12). Most of the calcium deposition happens in the hot ponds, which indeed are identified

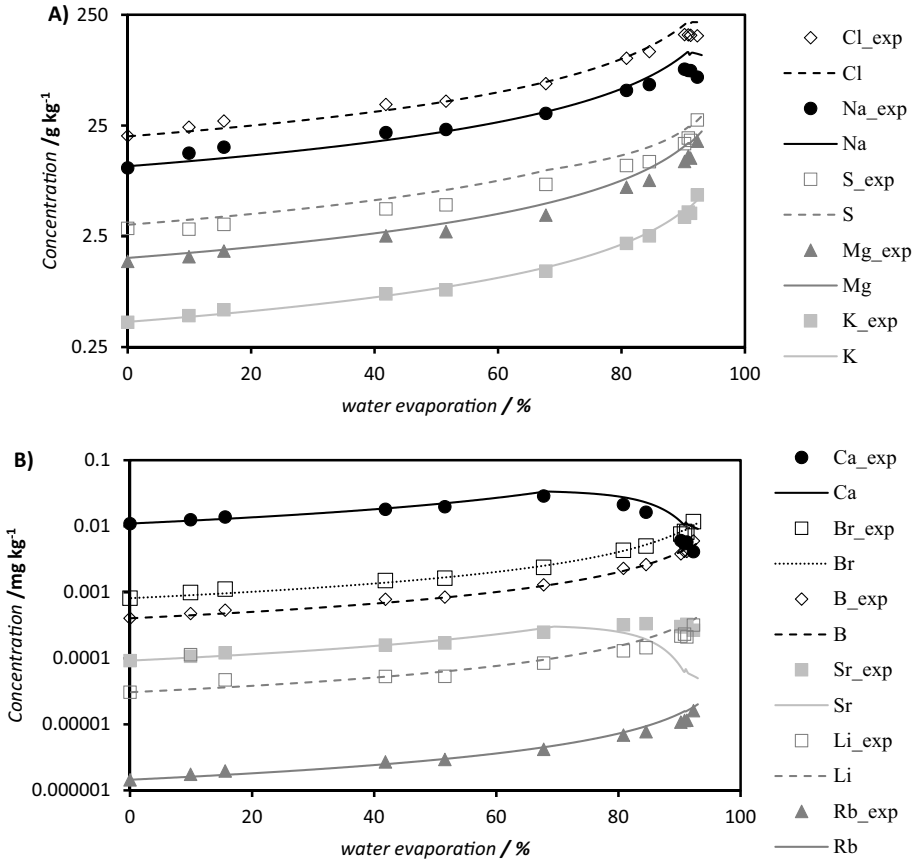

Fig. 6. Experimental (symbols) and modelling (lines) values for A) Major ion concentration (g/kg) and B) Minor ions concentration (mg/kg) during evaporation in Trapani saltworks.

by saltworkers for the removal of this mixture of minerals, historically used to build the walkways surrounding the salterns.

PHREEQC results were used to analyze the expected composition of the minerals crystallized in the last evaporation ponds as shown in Fig. 7 where the amount of salts produced (in form of g/Kg brine) is reported as a function of the concentration factor. As a result, gypsum crystallizes at CF values below 10, and keeps crystallizing further during halite deposition starting from CF values above 10. Indeed, it is one of the main impurities found in the table-salt along with magnesium salts such as epsomite ($MgSO_4$:$7H_2O_{(s)}$) starting its precipitation at CFs above 57. The simulation also describes the formation of other minerals as bloedite ($Na_2Mg(SO_4)_2$:$4\ H_2O_{(s)}$), for CF above 42, and polyhalite ($K_2MgCa_2(SO_4)_4$:$2\ H_2O_{(s)}$), for CFs above 30, as it could be seen in Fig. 7B. The formation of calcite and celestite is predicted for CF values below 12 where halite has not yet started its crystallization. The results obtained were in agreement with the solid analysis, showing that the precipitation of calcite occurs until pond 9 (CF ≈ 10), while gypsum precipitated from pond 6 to 11 (3.1 < CF < 10.5) (see Table 2 and Fig. 3).

Actually, these last magnesium containing salts are considered to be desired constituents making possible to respect the quality standard for the Protected Geographical Indication (PGI) mark of Trapani table salt (*Sale marino di Trapani*, IT/PGI/0005/00892). The relevance of magnesium bearing salts is further highlighted in Fig. 8, where all the minerals crystalizing in the saltworks are reported together in terms of relative mass percentage.

In Fig. 8, the *crystallization ponds area* is explicitly identified as the region within the horizontal curly bracket grouping all the points with CF between about 11 and 70. If all the solids produced in this area of the figure labelled as "crystallization pond area" are summed together (considering hence the average salt composition), it can be calculated that the salt produced is having a 98.27 % of halite (see in the Fig. S4 in the supplementary information file) when the abovementioned recirculation ratio (REC) is taken into account.

Indeed, as previously described, the Trapani saltworks operation is organized in such a way that NaCl saturated brine is mixed with more diluted water before accessing the crystallization ponds. The effect of the magnitude of this mixing on the purity of the salt produced was investigated and reported in the Fig. S5 in the supplementary information file, where also an estimation of the NaCl purity recovered in the final pond considering the amount of the different minerals formed as a function of the recirculation ratio is given. Accordingly, results indicate that PHREEQC code can represent a valuable tool to be used for operation planning, especially if brines blending options are a relevant stage on the operation of the ponds.

3.3. Saltworks brines as alternative option for critical raw materials recovery

Critical raw materials recovery from seawater has been initially focused on seawater reverse osmosis desalination brines and less on saltwork bitterns. However, looking at the Mediterranean region, the potential associated to saltwork brines is much larger than in other regions in the world due to the ancient history of most of the saltwork sites.

As it has been demonstrated in this study, even if large concentration factors are achieved along the evaporation ponds (CF > 50, see Fig. 8) the concentration of the target elements in the liquid phase is still in the order of mg/kg for the case of B, Sr, Li and Rb (see Fig. 7B). The predictive capacity of PHREEQC for this group of elements was excellent and could be used to model the concentration and separation stages, as most of the potential ways to recover B, Li and Rb are associated to high soluble minerals such as $LiOH_{(s)}$ and $Li_2CO_{3(s)}$ for Li(I), $RbCl_{(s)}$, $RbOH_{(s)}$ or $Rb_2SO_{4(s)}$ for Rb (I), $H_3BO_{3(s)}$ and $Na_2B_4O_7$:$12H_2O_{(s)}$ for B(III). On the other hand, the recovery of elements forming more insoluble mineral phases might be better implemented as a preliminary recovery step. A notable example, is Sr(II) which might be easily recovered as $SrSO_4$(s).

For other trace elements in μg/kg levels, such as Cs, Co, Ge and Ga, the recovery options from the liquid phase result to be challenging, as the extraction and concentration steps would require highly selective sorbents. Limited efforts were devoted to PHREEQC modelling of these elements so far, due to their very low concentration, near the detection limit. Additionally, most of the expected mineral phases have limited data for Pitzer and

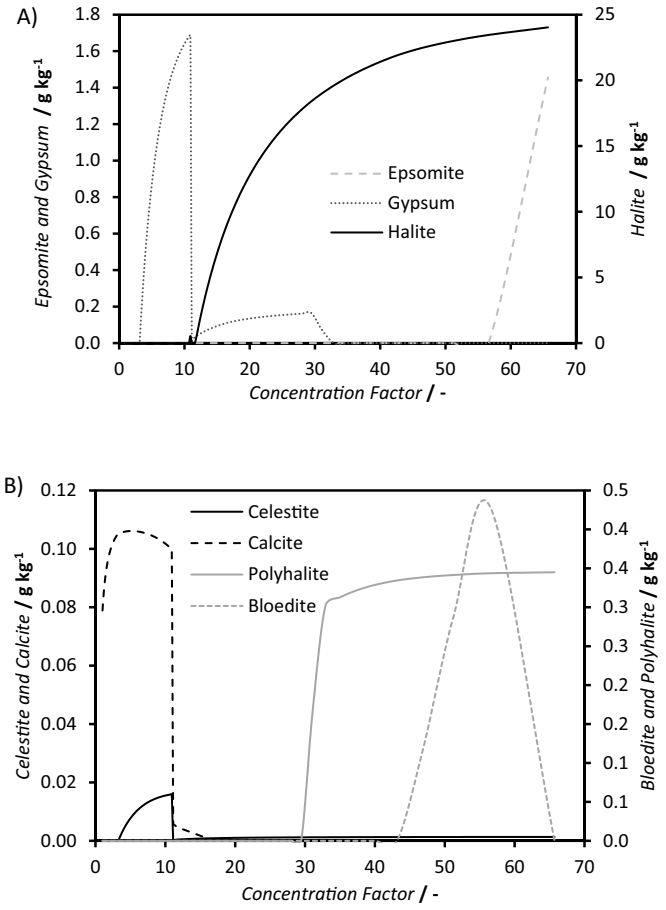

Fig. 7. PHREEQC simulation of minerals crystallization during seawater evaporation in Trapani saltworks. A) Major (>1 g/kg) and B) Minor (<1 g/kg) salts production for unit mass of seawater feed as a function of the concentration factor.

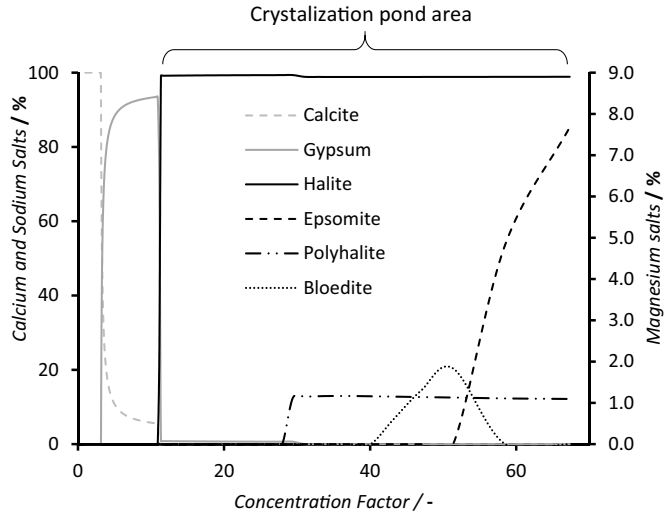

Fig. 8. PHREEQC simulation of minerals crystallization during seawater evaporation in Trapani saltworks in terms of sodium, calcium and magnesium minerals weight percentages.

solubility coefficients in the expected pH range of saltworks ponds, mainly $Co(OH)_{(s)}$, for Co(II), $GeO_{2(s)}$ for Ge(IV) and $CsCl_{(s)}$ or $Cs_2SO_{4(s)}$ for Cs(I).

In the case of Ga, a very wide-spread trace element with a content in the lithosphere of about 10 mg/kg, concentrations were one order of magnitude higher in comparison to Ge, Co and Cs, reaching a value of 0.013 mg/kg in P8 (see Table 1). From a mineralogy point of view, Ga is recognized by its inability to form its own minerals in natural geochemical conditions and considered as quite rare (Połedniok, 2008). Given the geochemical affinity between Al and Ga, the latter occurs mainly concentrated in: i) aluminium oxides being bauxites the main mineral in the nature and ii) hosted by aluminosilicates such as clays, apatites, nephelines and frequently alunite. Bauxite ores are the primary sources for Ga production, in fact approximately 90 % of world primary Ga is produced from leaching solutions of Bayer process (Gladyshev et al., 2015). Results of the mineralogical analysis of sludge samples collected along the ponds (see Table 2) identified different aluminosilicates as illite, kaolinite, microcline, montmorillonite and ankerite. EDAX analysis of such aluminosilicates did not detected the presence of Ga on the mineral particles as the typical contents are below of the limit of detection.

As it was predicted in the modelling stage, Sr(II) fate along the ponds has shown a non-conservative behavior precipitating in the last stages of the evaporation processes. This could be observed when analyzing the Sr (II) on the precipitates in ponds P5-P6 with values up to 1.7 mg/kg and latter reaching values up to 3 mg/kg in the last ponds. Removal and precipitation was well described by formation of celestite, however, as described in the literature (Molinari et al., 2021), precipitation of calcite in brines is kinetically favored by the presence of Sr(II) and Mg(II). The substitution of Ca (II) cations by Sr(II) and Mg(II) ions is more favored in the aragonite crystal structure than in calcite. Formation of calcite is controlled by different chemical parameters as pH of the brine, Ca(II) and total bicarbonate concentration and as well as physical parameters as temperature, evaporation and biological processes. When analyzing the fate of Ca(II) along the ponds its concentration is controlled by the evaporation ratio and the formation of calcite at the lower evaporation rates and gypsum at the higher evaporation rates as described in Fig. 7. The associated molar enthalpy for the calcite dissolution reaction (ΔH^{o}_{so}), with negative values in the expected temperature range (e.g. form -5 kJ/mol at 5 °C up to -24.7 kJ/mol at 60 °C), indicates that lower solubility values, and then lower Ca(II) concentrations values are expected at the ponds with the higher temperatures. However, the small changes associated with the calcite solubility constant along the temperature ranges ($\log K_{so}(5\,^{\circ}C) = -8.2$ and $\log K_{so}(60\,^{\circ}C) = -8.6$) implies that the potential changes associated to precipitation and re-dissolution of calcite due to temperature variations are having a limited effect when compared with the changes associated to the evaporation processes. The contribution of both factors (temperature and evaporation ratio) on the solubility of calcite has been modeled using PHREEQC. As it shown in Fig. S6 (supplementary information), the influence of temperature on calcite solubility only is more relevant with differences of up to 20 % at the lower evaporation rates (e.g. first ponds) and being neglectable when the evaporation rates are much higher than 70 %.

4. Conclusions

In the present work, the mechanism governing fractionated separation of minerals during seawater evaporation has been unveiled combining measured compositions of liquid and solid samples along the saltworks ponds and the set of equilibrium data and Pitzer parameters to model the main physic-chemical processes taking place along the evaporation ponds. With this respect, Pitzer database was properly extended, including for the first time elements conventionally neglected for their low content, such as Sr, Cs, Rb, Co, Ga and Ge.

PHREEQC code incorporating the Pitzer model was providing a good description of the fate of the major and minor ions present in the saltworks brine. Minerals precipitation path was properly reproduced including the known major ions sequence and the less minor ions with very high correlation for ionic composition ($0.9 < R^2 < 0.99$).

The concentration factor during seawater evaporation that can cause calcium and magnesium fractionated crystallization in the form of carbonates and sulphates was identified and compared against the composition of liquid samples and SEM, EDS and XRD of the solids. A progress in the state-of-the-art knowledge in minerals separation has been achieved, as for the first-time strontium, a trace element belonging to the list of critical raw materials, was predicted to be separated in the form of celestite and identified in the crystals deposited at the bottom of a pond.

The results obtained pose a fundamental step in CRMs mining from seawater brine, opening new possibilities for process optimization and intensification. Similarly, the approach developed can be adopted for the study of other thermal or membrane processes aiming at CRMs recovery from different brines.

Finally, a natural application of the platform developed is the assessment of possible long-term effect of desalination brine integration into saltworks ponds, such as productivity increase and purity loss. In fact, this tool can also allow to design alternate water path and flow recirculation than can prevent quality loss and maximize purity even for the case of desalination brine integration.

CRediT authorship contribution statement

Conceptualization, A.C., F.V., J.L., J.L.C. and S.R.;
Methodology, M.F., V·V., J.L., J.L.C., S.R., A.C., and F.V.;
Software, F.V. and J.L.;
Validation, J.L.C., G.D.S. and A.C.;
Formal analysis, F.V. and J.L.;
Investigation, M.F., V.V. and J.L.;
Resources, G.D.S.;
Data curation, F.V., J.L., M.F. and S.R.;
Writing—original draft preparation, F.V., S.R., J.L.;
Writing—review and editing, A.C., A.T., J.L.C. and G.D.S.;
Visualization, F.V., S.R. and J.L.C.;
Supervision, A.C., J.L.C. and A.T.;
Project administration, G.M., A.C. and A.T.;
Funding acquisition, G.M. and A.C.

All authors have read and agreed to the published version of the manuscript.

Declaration of competing interest

The authors declare that they have no known competing financial interests or personal relationships that could have appeared to influence the work reported in this paper.

Acknowledgements

This work was supported by the EU within SEArcularMINE (Circular Processing of Seawater Brines from Saltworks for Recovery of Valuable Raw Materials) project – Horizon 2020 programme, Grant Agreement no. 869467. This output reflects only the author's view. The European Health and Digital Executive Agency (HaDEA) and the European Commission cannot be held responsible for any use that may be made of the information contained therein.

Sosalt saltworkers Giuseppe and Giovanni Culcasi are thankfully acknowledged for sharing their ancestral knowledge with the SEArcularMINE project. Dr. C. Ayora from IDAEA-CSIC (Barcelona, Spain) is acknowledged for his help on the review of the PHREEQC Pitzer data base completion and guidance on the modelling stage and on the discussion and results interpretation of the mineralogical data from the solid samples collected on the bottom parts of the ponds.

Appendix A. Supplementary data

Supplementary data to this article can be found online at https://doi.org/10.1016/j.scitotenv.2022.157544.

References

Anirudhan, T.S., Lekshmi, G.S., Shainy, F., 2019. Synthesis and characterization of amidoxime modified chitosan/bentonite composite for the adsorptive removal and recovery of uranium from seawater. J. Colloid Interface Sci. 534, 248–261. https://doi.org/10.1016/j.jcis.2018.09.009.

Bąbel, M., Schreiber, B.C., 2014. Geochemistry of Evaporites and Evolution of Seawater, Treatise on Geochemistry. Second edition. https://doi.org/10.1016/B978-0-08-095975-7.00718-X.

Bae, H., Kim, Y., 2021. Technologies of lithium recycling from waste lithium ion batteries: a review. Mater. Adv. 2, 3234–3250. https://doi.org/10.1039/d1ma00216c.

Barbier, J., Levy, D., 2010. ChemInform abstract: $Pb_2Fe_2Ge_2O_9$, the germanate analogue of the silicate mineral melanotekite. ChemInform 29. https://doi.org/10.1002/chin.199816006 no-no.

Bardi, U., 2010. Extracting minerals from seawater: an energy analysis. Sustainability 2, 980–992. https://doi.org/10.3390/su2040980.

Butterman, W.C., Reese, R.G., 2003. Mineral Commodity Profiles Rubidium. U.S. Geol. Surv. Open-File Rep. 03-045, pp. 1–11 https://doi.org/10.3133/ofr0345.

Cipollina, A., Micale, G., 2016. Sustainable energy from salinity gradients. Sustainable Energy from Salinity Gradients, First edit. Woodhead Publishing, Elsevier, Amsterdam https://doi.org/10.1016/C2014-0-03709-4.

Cipollina, A., Misseri, A., Staiti, G.D.A.D., Galia, A., Micale, G., Scialdone, O., 2012. Integrated production of fresh water, sea salt and magnesium from sea water. Desalin. Water Treat. 49, 390–403. https://doi.org/10.1080/19443994.2012.699340.

Cipollina, A., Bevacqua, M., Dolcimascolo, P., Tamburini, A., Brucato, A., Glade, H., Buether, L., Micale, G., 2015. Reactive crystallisation process for magnesium recovery from concentrated brines. Desalin. Water Treat. 55, 2377–2388. https://doi.org/10.1080/19443994.2014.947771.

Coelho, Ricardo, J., Hillario, Mauro, R., Duarte, Nuno, R., 2014. Solar salt works integrated management. Sol. Salt Work. Econ. Value Biodivers. 58–65.

Davis, J.S., 2013. Structure, function and management of the biological system for seasonal solar saltworks. Glob. NEST J. 2, 217–226. https://doi.org/10.30955/gnj.000175.

European Commission, 2020. Study on the review of the list of critical raw materials - final report. Critical Raw Materials Factsheets https://doi.org/10.2873/11619.

Froelich, P.N., Hambrick, G.A., Andreae, M.O., Mortlock, R.A., Edmond, J.M., 1985. The geochemistry of inorganic germanium in natural waters. J. Geophys. Res. 90, 1133. https://doi.org/10.1029/JC090iC01p01133.

Gabitov, R.I., Sadekov, A., Dyer, J., Perez-Huerta, A., Xu, H., Migdisov, A., 2021. Sectoral and growth rate control on elemental uptake by individual calcite crystals. Chem. Geol. 585, 120589. https://doi.org/10.1016/j.chemgeo.2021.120589.

Gamazo, P., Bea, S.A., Saaltink, M.W., Carrera, J., Ayora, C., 2011. Modeling the interaction between evaporation and chemical composition in a natural saline system. J. Hydrol. 401, 154–164. https://doi.org/10.1016/j.jhydrol.2011.02.018.

Gao, D., Li, D., Hu, B., Li, W., 2020. Solid-aqueous phase equilibria in the quaternary NaCl + KCl + RbCl + H_2O system: thermodynamic predictions and experimental verifications at 298.15 K. J. Chem. Eng. Data 65, 4837–4844. https://doi.org/10.1021/acs.jced.0c00384.

Gladyshev, S.V., Akcil, A., Abdulvaliyev, R.A., Tastanov, E.A., Beisembekova, K.O., Temirova, S.S., Deveci, H., 2015. Recovery of vanadium and gallium from solid waste by-products of Bayer process. Miner. Eng. 74, 91–98. https://doi.org/10.1016/j.mineng.2015.01.011.

Glavaš, N., Défarge, C., Gautret, P., Joulian, C., Penhoud, P., Motelica, M., Kovač, N., 2018. The structure and role of the "petola" microbial mat in sea salt production of the Sečovlje (Slovenia). Sci. Total Environ. 644, 1254–1267. https://doi.org/10.1016/j.scitotenv.2018.07.009.

Golan, R., Gavrieli, I., Ganor, J., Lazar, B., 2016. Controls on the pH of hyper-saline lakes – a lesson from the Dead Sea. Earth Planet. Sci. Lett. 434, 289–297. https://doi.org/10.1016/j.epsl.2015.11.022.

Hajbi, F., Hammi, H., M'Nif, A., 2010. Reuse of RO desalination plant reject brine. J. Phase Equilibria Diffus. 31, 341–347. https://doi.org/10.1007/s11669-010-9727-3.

Hajbi, F., Hammi, H., Solimando, R., M'nif, A., 2016. Thermodynamic study of magnesium sulfate crystallization: application of Pitzer model and quinary diagrams. Desalin. Water Treat. 57, 18248–18259. https://doi.org/10.1080/19443994.2015.1089419.

Hirotsu, T., Katoh, S., Sugasaka, K., Sen?, M., Itagaki, T., 1986. Adsorption equilibrium of uranium from aqueous $[UO_2(CO_3)_3]^{4-}$ solutions on a polymer bearing amidoxime groups. J. Chem. Soc. Dalt. Trans. 1983. https://doi.org/10.1039/dt9860001983.

Kasedde, H., Kirabira, J.B., Bäbler, M.U., Tilliander, A., Jonsson, S., 2014. Characterization of brines and evaporites of Lake Katwe, Uganda. J. African Earth Sci. 91, 55–65. https://doi.org/10.1016/j.jafrearsci.2013.12.004.

Kolpakova, M.N., Gaskova, O.L., 2018. Major ions behaviour during evaporation of different saline type water of Western mongolian lakes (geochemical modelling). Hydrol. Res. 49, 163–176. https://doi.org/10.2166/nh.2017.148.

Li, D., Zeng, D., Yin, X., Han, H., Guo, L., Yao, Y., 2016. Phase diagrams and thermochemical modeling of salt lake brine systems. II. NaCl + H_2O, KCl + H_2O, $MgCl_2$ + H_2O and $CaCl_2$ + H_2O systems. Calphad Comput. Coupling Phase Diagrams Thermochem. 53, 78–89. https://doi.org/10.1016/j.calphad.2016.03.007.

Li, D., Liu, Y., Meng, L., Guo, Y., Deng, T., Yang, L., 2019. Phase diagrams and thermodynamic modeling of solid-liquid equilibria in the system NaCl–KCl–$SrCl_2$–H_2O and its application in industry. J. Chem. Thermodyn. 136, 1–7. https://doi.org/10.1016/j.jct.2019.04.013.

Loganathan, P., Naidu, G., Vigneswaran, S., 2017. Mining valuable minerals from seawater: a critical review. Environ. Sci. Water Res. Technol. 3, 37–53. https://doi.org/10.1039/c6ew00268d.

Lorens, R.B., 1981. Sr, cd, mn and co distribution coefficients in calcite as a function of calcite precipitation rate. Geochim. Cosmochim. Acta 45, 553–561. https://doi.org/10.1016/0016-7037(81)90188-5.

Macedonio, F., Drioli, E., 2017. Advanced membrane-based desalination systems for water and minerals extracted from the sea. Desalin. Sustain. A Tech. Socioecon. Environ. Approach, 237–259 https://doi.org/10.1016/B978-0-12-809791-5.00006-7.

Macedonio, F., Quist-Jensen, C.A., Al-Harbi, O., Alromaih, H., Al-Jlil, S.A., Al Shabouna, F., Drioli, E., 2013. Thermodynamic modeling of brine and its use in membrane crystallizer. Desalination 323, 83–92. https://doi.org/10.1016/j.desal.2013.02.009.

Marazuela, M.A., Vázquez-Suñé, E., Custodio, E., Palma, T., García-Gil, A., Ayora, C., 2018. 3D mapping, hydrodynamics and modelling of the freshwater-brine mixing zone in salt flats similar to the Salar de Atacama (Chile). J. Hydrol. 561, 223–235. https://doi.org/10.1016/j.jhydrol.2018.04.010.

Millero, F.J., Feistel, R., Wright, D.G., McDougall, T.J., 2008. The composition of standard seawater and the definition of the reference-composition salinity scale. DeepRes. Part I Oceanogr. Res. Pap. 55, 50–72. https://doi.org/10.1016/j.dsr.2007.10.001.

Molinari, R., Avci, A.H., Argurio, P., Curcio, E., Meca, S., Plà-Castellana, M., Cortina, J.L., 2021. Selective precipitation of calcium ion from seawater desalination reverse osmosis brine. J. Clean. Prod. 328, 129645–129655. https://doi.org/10.1016/j.jclepro.2021.129645.

Muuri, E., Ikonen, J., Matara-Aho, M., Lindberg, A., Holgersson, S., Voutilainen, M., Siitari-Kauppi, M., Martin, A., 2020. Behavior of cs in grimsel granodiorite: sorption on main minerals and crushed rock. Radiochim. Acta 04, 575–582. https://doi.org/10.1515/RACT-2016-2574.

Nir, O., Marvin, E., Lahav, O., 2014. Accurate and self-consistent procedure for determining pH in seawater desalination brines and its manifestation in reverse osmosis modeling. Water Res. 64, 187–195. https://doi.org/10.1016/j.watres.2014.07.006.

Parkhurst, D.L., Appelo, C.A.J., 2013. Description of Input and Examples for PHREEQC Version 3 — A Computer Program for Speciation, Batch-reaction, One-dimensional Transport, and Inverse Geochemical Calculations. U.S. Geological Survey Techniques and Methods, Book 6, Chapter A43 497 p. U.S. Geol. Surv. Tech. Methods, B. 6, chapter A43 6-43A.

Pitzer, K.S., 1981. The treatment of ionic solutions over the entire miscibility range. Berichte der Bunsengesellschaft für Phys. Chemie 85, 952–959. https://doi.org/10.1002/bbpc.19810851107.

Pokrovsky, O.S., Pokrovski, G.S., Schott, J., Galy, A., 2006. Experimental study of germanium adsorption on goethite and germanium coprecipitation with iron hydroxide: X-ray absorption fine structure and macroscopic characterization. Geochim. Cosmochim. Acta 70, 3325–3341. https://doi.org/10.1016/j.gca.2006.04.012.

Połedniok, J., 2008. Speciation of scandium and gallium in soil. Chemosphere 73, 572–579. https://doi.org/10.1016/j.chemosphere.2008.06.012.

Pramanik, B.K., Nghiem, L.D., Hai, F.I., 2020. Extraction of strategically important elements from brines: constraints and opportunities. Water Res. 168, 115149. https://doi.org/10.1016/j.watres.2019.115149.

Reeder, R.J., 1996. Interaction of divalent cobalt, zinc, cadmium, and barium with the calcite surface during layer growth. Geochim. Cosmochim. Acta 60, 1543–1552. https://doi.org/10.1016/0016-7037(96)00034-8.

Sainz-López, N., Boski, T., Sampath, D.M.R., 2019. Fleur de sel composition and production: analysis and numerical simulation in an artisanal saltern. J. Coast. Res. 35, 1200–1214. https://doi.org/10.2112/JCOASTRES-D-18-00132.1.

SEArcularMINE, 2021. No Title [WWW Document]. website. http://www.searcularmine.eu (accessed 5.6.21).

Simonson, J.M., Pitzer, K.S., 1986. Thermodynamics of multicomponent, miscible ionic systems: the system lithium nitrate-potassium nitrate-water. J. Phys. Chem. 90, 3009–3013. https://doi.org/10.1021/j100404a043.

Spooren, J., Binnemans, K., Björkmalm, J., Breemersch, K., Dams, Y., Folens, K., González-Moya, M., Horckmans, L., Komnitsas, K., Kurylak, W., Lopez, M., Mäkinen, J., Onisei, S., Oorts, K., Peys, A., Pietek, G., Pontikes, Y., Snellings, R., Tripiana, M., Varia, J., Willquist, K., Yurramendi, L., Kinnunen, P., 2020. Near-zero-waste processing of low-grade, complex primary ores and secondary raw materials in Europe: technology development trends. Resour. Conserv. Recycl. 160, 104919. https://doi.org/10.1016/j.resconrec.2020.104919.

Vančina, V., Kester, D.R., Bilinski, H., 1997. Application of the pitzer model to solar salt brine chemistry. Croat. Chem. Acta 70, 55–69.

Wang, C., Yu, Y., Chen, Y., Cao, M., Wang, J., Yang, X., Qiu, S., Wei, D., Gao, H., Li, F., 2021. Efficient quantum memory of orbital angular momentum qubits in cold atoms. Quantum Sci. Technol. 6, 045008. https://doi.org/10.1088/2058-9565/ac120a.

Zhu, T., Dittrich, M., 2016. Carbonate precipitation through microbial activities in natural environment, and their potential in biotechnology: a review. Front. Bioeng. Biotechnol. 4, 1–21. https://doi.org/10.3389/fbioe.2016.00004.